Received: 15 November 2023 | Revised: 21 March 2024 | Accepted: 25 March 2024

DOI: 10.1111/ejn.16341

RESEARCH REPORT

EJN European Journal of Neuroscience FENS WILEY

Association cortical areas in the mouse contain a large population of fast-spiking GABAergic neurons that do not express parvalbumin

Erik Justin Courcelles | Kasper Kjelsberg | Laura Convertino | Rajeevkumar Raveendran Nair | Menno P. Witter | Maximiliano José Nigro

Kavli Institute for Systems Neuroscience, Center for Algorithms in the Cortex, Egil and Pauline Braathen and Fred Kavli Center for Cortical Microcircuits, Norwegian University of Science and Technology, Trondheim, Norway

Correspondence
Maximiliano José Nigro, Kavli Institute for Systems Neuroscience, Center for Algorithms in the Cortex, Egil and Pauline Braathen and Fred Kavli Center for Cortical Microcircuits, Norwegian University of Science and Technology, Trondheim, Norway.
Email: maximiliano.j.nigro@ntnu.no

Funding information
Norwegian Research Council, Grant/Award Numbers: 223262, 332640; European Union's Horizon 2020 Research and Innovation Programme, Grant/Award Number: 885955; Kavli Foundation

Edited by: Gianmaria Maccaferri

Abstract

GABAergic neurons represent 10–15% of the neuronal population of the cortex but exert a powerful control over information flow in cortical circuits. The largest GABAergic class in the neocortex is represented by the parvalbumin-expressing fast-spiking neurons, which provide powerful somatic inhibition to their postsynaptic targets. Recently, the density of parvalbumin interneurons has been shown to be lower in associative areas of the mouse cortex as compared with sensory and motor areas. Modelling work based on these quantifications linked the low-density of parvalbumin interneurons with specific computations of associative cortices. However, it is still unknown whether the total GABAergic population of association cortices is smaller or whether another GABAergic type can compensate for the low density of parvalbumin interneurons. In the present study, we investigated these hypotheses using a combination of neuroanatomy, mouse genetics and neurophysiology. We found that the GABAergic population of association areas is comparable with that of primary sensory areas, and it is enriched of fast-spiking neurons that do not express parvalbumin and were not accounted for by previous quantifications. We developed an intersectional viral strategy to demonstrate that the population of fast-spiking neurons is comparable across cortical regions. Our results provide quantifications of the density of fast-spiking GABAergic neurons and offers new biological constrains to refine current models of cortical computations.

Abbreviations: A35, Area 35; A36, Area 36; AAV, adenoassociated virus; AHP_{dur}, afterhyperpolarization duration; AP, antero-posterior; AP_{HW}, action potential half-width; AP_{thr}, action potential threshold; CGE, caudal ganglionic eminence; DV, dorso-ventral; ECT, ectorhinal cortex; fAHP, fast afterhyperpolarization; F_{Max}, maximal firing frequency; GFP, green fluorescent protein; IL, infralimbic cortex; INT, interneuron; IR, input resistance; LEC, lateral entorhinal cortex; MGE, medial ganglionic eminence; ML, medio-lateral; NGS, normal goat serum; PB, phosphate buffer; PBS, phosphate buffer saline; PCA, principal component analysis; PER, perirhinal cortex; PFA, paraformaldehyde; PrL, prelimbic cortex; PV, parvalbumin; Rheo, rheobase; ROI, region of interest; SST, somatostatin; V1, primary visual cortex; VIP, vasoactive intestinal peptide; wS1, whisker representation primary somatosensory cortex.

KEYWORDS
cerebral cortex, inhibitory interneurons, parvalbumin, perirhinal cortex, prefrontal cortex

1 | INTRODUCTION

The wide neuronal diversity of the cerebral cortex is thought to endow it with a variety of circuit motifs that shape information processing (Harris & Shepherd, 2015; Luo, 2021). The cerebral cortex can be parcellated into functional areas that show specific cytoarchitectonic features and expression of molecular markers (Van Essen & Glasser, 2018). The relationship between cortical parcellation and distribution of neuron types in the cortex is poorly understood. Recent studies unveiled a correlation between the distribution of GABAergic types and the connectivity-based hierarchical organization of the cortex (Ding et al., 2024; Kim et al., 2017). GABAergic neurons represent 10–15% of the neuronal population, and their diversity allows them to participate in different cortical microcircuits (Kepecs & Fishell, 2014; Tremblay et al., 2016). GABAergic neurons are divided in two major groups according to embryonal origin: those derived from the medial ganglionic eminence (MGE) and those derived from the caudal ganglionic eminence (CGE) (Rudy et al., 2011). MGE-derived GABAergic neurons are further divided according to molecular marker expression into parvalbumin (PV)-expressing and somatostatin (SST)-expressing interneurons (INs) (Tremblay et al., 2016). CGE-derived INs (CGE-INs) have been divided in VIP-expressing and VIP non-expressing neurons (Lee et al., 2010). Transcriptomic analysis has confirmed this classification and further divided the CGE group into three major classes: vasoactive intestinal peptide (VIP)-expressing, Lamp5 and Sncg groups (Tasic et al., 2018).

Molecularly defined GABAergic neurons have been shown to be homogeneously distributed across sensory-motor areas of the neocortex (Xu et al., 2010). However, recent cortex-wide examination of the distribution of three major GABAergic groups (PV, SST, VIP) revealed a reduction of the density of PV-INs in association cortices (Kim et al., 2017; Whissell et al., 2015). PV-INs are the most abundant GABAergic type in the neocortex; they show a characteristic fast-spiking firing pattern and provide powerful perisomatic inhibition to their postsynaptic targets (Tremblay et al., 2016). In sensory cortices, PV-INs participate in feedforward inhibitory circuits gating information flow in the thalamocortical circuit and in translaminar circuits (Gabernet et al., 2005; Helmstaedter et al., 2008; Pouille & Scanziani, 2001). In association cortices, PV-INs have been shown to receive long-range excitatory inputs and have been shown to mediate feedforward inhibition (Anastasiades et al., 2018; McGarry & Carter, 2016; Willems et al., 2018). Their role in sensory gating through feedforward inhibition led to the hypothesis that PV-INs control the flow of sensory information in the cortico-hippocampal network (De Curtis & Paré, 2004; Willems et al., 2018). This is in striking contrast with the low density of PV-INs in association areas described previously (Kim et al., 2017; Whissell et al., 2015). The low density of PV-INs suggests that either the GABAergic population of association areas is smaller than that of the sensory-motor areas or that other GABAergic cell-types are enriched. In the present study, we aimed to explore these two scenarios by combining mouse genetics, molecular marker expression, viral-mediated enhancer driven transgene expression and electrophysiological characterization of GABAergic neurons in the cortex. We found that indeed the GABAergic population of association areas is not smaller than in sensory cortices, suggesting an enrichment of other IN types. We identified a large group of fast-spiking neurons that do not express PV in association cortex and developed an intersectional viral approach to label them, which allowed us to show that the density of fast-spiking neurons is comparable across cortical regions.

Our results unveiled the presence of a large GABAergic population that was not accounted for because of the lack of markers and tools for labelling it. Our study provides new constrains to guide future modelling work of the computational abilities of different cortical regions.

2 | MATERIALS AND METHODS

2.1 | Animal models

The research described here was performed on adult mice (>8 weeks old) of both sexes. We used the following mouse lines from Jackson Laboratories: C57BL/6J mice ($n = 6$) (stock 000664), SST-Cre mice ($n = 6$) (stock 013044). The GAD67-GFP mice ($n = 23$) were obtained as gift from Dr. Yanagawa (Tamamaki et al., 2003). The

GAD67-GFP and SST-cre mice were bred as heterozygous. Animals were bred in house, group housed in enriched cages with water and food ad libitum. Animals were kept with an inverted dark/light cycle of 12 h/12 h. All procedures described were approved by the Norwegian Food Authority (application number 25405).

2.2 | Adeno-associated virus (AAV) production

Viral vectors were produced by the Viral Vector Core Facility at the Kavli Institute for Systems Neuroscience at NTNU. For producing AAV1-S5E2-dTom (S5E2-dTom), the plasmid construct pAAV-S5E2-dTom was purchased from Addgene (#135630) (Vormstein-Schneider et al., 2020). For AAV1-S5E2-lox2272 dTom loxP- reverse complement (rc)GFP lox2272 loxp (S5E2-*lox* dTom *lox* rcGFP *lox2*), first we synthesized the corresponding gene segments and cloned in the pAAV-S5E2-dTom plasmid backbone as described below. Briefly, using NheI and EcoRV restriction sites in pAAV-S5E2-dTom plasmid, we cloned in the sequence of nls-dTomato flanked by incompatible lox2272 and loxP sites followed by reverse complement sequence of green fluorescent protein (GFP) followed by two lox sites lox2272 and loxP sites at the 3′ end. This arrangement of lox sites and gene sequences driven by S5E2 promoter in S5E2-*lox* dTom *lox* rcGFP *lox2* enables the expression of dTomato in E2/SST Cre− cells, whereas the expression of GFP only after Cre-mediated recombination (in E2/SST Cre+ cells).

S5E2-*lox* dTom *lox* rcGFP *lox2* was packaged in AAV1 and purified using iodixanol density gradient method. Specifically, the corresponding pAAV plasmid construct along with AAV helper plasmids encoding the structural elements was transfected using polyethylenimine (PEI) into the AAV-293 cell line (CVCL_6871, Agilent, USA). The day before transfection, 7×10^6 AAV-293 cells were seeded into 150-mm cell culture plates in DMEM (# 41965062, Thermo Fisher Scientific) containing 10% fetal bovine serum (FBS) (#16000-044, ThermoFisher, USA) and penicillin/streptomycin antibiotics (#15140122, Thermo Fisher Scientific). All the plasmids for AAV vector preparations were made using endotoxin free plasmid maxiprep kit (#12663, Qiagen). PEI mediated co-transfection of pAAV plasmid-containing the transgene, pHelper and pAAV1 capsid helper plasmids were carried out on next day. After 24 h, the medium was replaced with fresh 10% FBS-containing DMEM. The AAV-293 cells were cultured for 2 days following transfection to allow AAV synthesis to occur in cells. The medium and AAV-293 cells filled with virus particles were scraped from the cell culture plates, then isolated by centrifugation at 200 × g. The cell pellet was then subjected to lysis using 20-mM Tris, 300-mM NaCl and 20-mM $MgCl_2$, pH 7.6 buffer. The supernatant was mixed with 40% Polyethylene Glycol 8000 (PEG) for 2 h in ice for precipitation of virus particles. The PEG treated medium was centrifuged at 4000 × g for 15 min. The lysate and the PEG-precipitate were treated with benzonase nuclease HC (#71206-3, Millipore) for 45 min at 37°C. Benzonase-treated lysate was centrifuged at 3000 × g for 15 mins, and the clear supernatant then subjected to iodixanol gradient ultracentrifugation. Four different layers of the gradient, that is, 15%, 25%, 40% and 58% of iodixanol, were built in a Beckman quick-seal centrifuge tube. Phenol red was added to the 25% and 58% layers to aid visualization of the layers within the tube. The virus containing supernatant was layered above the 15% iodixanol by slowly dripping the solution onto the top layer of the gradient. Seal the tip of the tube using a heating device (Beckman and Coulter). Sealed tubes were centrifuged at 350,000 g for 90 min in a T70i rotor at 10°C. The 40% iodixanol layer after ultracentrifugation was collected and buffer exchanged with DPBS using Amicon Ultra centrifugal filters (#Z648043, Millipore) (modified protocol from Addgene, USA). We performed quantitative polimerase chain reaction (PCR) on the viral stocks, and the titre was determined as approximately 1.9×10^{12} genomic copies/ml for S5E2-*lox* dTom *lox* rcGFP *lox2*.

2.3 | Injections of viral vectors

The AAVs were injected into the brains of C57 ($n = 6$) and SST-cre ($n = 3$) mice. Mice were anaesthetized with isoflurane (4% Nycomed, airflow 1 L/min) in an induction chamber. The mice were placed in a stereotactic frame on a heated pad (37°C) throughout the procedure and head-fixed with ear bars. Eye ointment was applied to protect the cornea. The following analgesics were applied subcutaneously: buprenorphine hydrochloride (.1 mg/kg, Temgesic, Invidior), meloxicam (1 mg/kg, Metacam Boerringer Ingelheim Vetmedica), bupivacaine hydrochloride (1 mg/kg locally, Marcain, Astra Zeneca). The skin on the incision site was shaved and disinfected with Pyrisept. An incision was made to access the skull. The skull was thinned with a dental drill at the desired location, and a hole was punched with the tip of a glass pipette. We used the following coordinates from bregma: for wS1–.7 mm AP, +3.1 mm ML, −.15 and −.55 DV; for PER/ECT −3 mm AP, −1.5 DV, for the ML the pipette was moved to the edge of the skull and then retracted medially .4 mm; for PrL/IL: +1.8 mm AP, .25 mm ML, −1.3 mm DV. Injections of 100–200 nl (50 nl/minute) in

each location were made with a glass pipette (20- to 30-μm tip size) attached to an injector (Nanoliter 2010, World Precision Instruments) controlled by a microsyringe pump controller (Micro4 pump, World Precision Instruments). After retracting the pipette, the wound was rinsed with saline and sutured. The mice were allowed to recover in a heated chamber (37°C) before returning to the homecage. Postoperative analgesic was applied 6–8 h after the procedure (Temgesic) and 24 h after the procedure (Metacam). The survival time for transduction and expression of the genetic material was 10–15 days.

2.4 | In vitro electrophysiology

Mice of either sex (>8 week old) were euthanized with an overdose of pentobarbital (i.p. 100 mg/kg, Apotekerforeninger), before intracardial perfusion with cutting solution (RT) of the following composition (in mM): 93 choline chloride, 3 KCl, 1.25 NaH_2PO_4, 30 $NaHCO_3$, 20 HEPES, 10 glucose, 5 $MgCl_2$, .5 $CaCl_2$, 5 N-acetylcysteine, saturated with 95% O_2 and 5% CO_2. The brain was extracted, and a section containing either PER or wS1 was glued onto the stage of a vibratome (VT1000, Leica) filled with cold (4°C) cutting solution. Slices (300 μm) were transferred to a chamber filled with warm (34°C) cutting solution and incubated for 15 min. The slices were stored in a different chamber filled with the following solution (in mM) (RT): 92 NaCl, 3 KCl, 1.25 NaH_2PO_4, 30 $NaHCO_3$, 20 HEPES, 10 glucose, 5 $MgCl_2$, .5 $CaCl_2$, 5 N-acetylcysteine, saturated with 95% O_2 and 5% CO_2.

The slices were placed in a recording chamber of an upright microscope (BW51, Olympus) filled with warm (35°C) recording solution of the following composition: 124 NaCl, 3 KCl, 1.25 NaH_2PO_4, 26 $NaHCO_3$, 10 glucose, 1 $MgCl_2$, 1.6 $CaCl_2$, saturated with 95% O_2 and 5% CO_2. Characterization of the electrophysiological properties was performed in presence of synaptic blockers: 10-μM $DNQXNa_2$, 25-μM APV and 10-μM gabazine. wS1 was identified under DIC optics by the presence of characteristic barrels in layer 4. To identify PER under DIC optics, we first identified the lateral entorhinal cortex (LEC) by its characteristic large neurons in layer 2a, and by the clear separation between layer 2a and 2b. PER was defined as the cortex dorsally located to LEC. Only healthy, fluorophore-expressing neurons were selected for recordings, and no other criterion was applied. Whole-cell patch clamp recordings were performed with borosilicate pipettes (Harvard Apparatus, Massachusetts, USA) with a resistance of 3–7 MΩ filled with a solution of the following composition (in mM): 130 K-gluconate, 10 KCl, 10 HEPES, .2 EGTA, 4 ATP-Mg, .3 GTP-Na, 5 phosphocreatine-Na2, pH 7.3. In all recordings, biocytin was added to the pipette solution to recover the layer location of the neuron. Membrane potentials reported were not corrected for a junction potential of −14 mV. Current clamp recordings were performed with a Multiclamp 700B amplifier (Molecular Devices), digitized with a 1550A Digidata (Molecular Devices), interfaced with a personal computer with pClamp 11 (Molecular Devices). Data were sampled at 40 kHz and low-passed filtered at 10 kHz. All recordings were performed from a holding potential of −65 mV. The electrophysiological parameters analysed were defined as follows:

Input resistance (IR, MΩ): resistance measured from Ohm's law from the peak of voltage responses to −25 pA hyperpolarizing current steps.

Sag ratio (dimensionless): measured from voltage responses peaking at -90 ± 2 mV to hyperpolarizing current steps. It is defined as the ratio between the voltage at the steady-state response and the peak.

Rheobase (Rheo, pA): current level that evoked the first spike during a 1-s-long depolarizing ramp (500 pA/s).

Action potential (AP) threshold (APthr, mV): measured from APs evoked near rheobase and defined as the voltage where the rise of the AP was 20 mV/ms.

AP half width (AP_{HW}, ms): duration of the AP at half amplitude from APthr, measured from APs evoked near rheobase.

Amplitude of the fast afterhyperpolarization (fAHP, mV): measured from APthr, from APs evoked near rheobase.

AHP duration (AHPdur, ms): measured from APs evoked near rheobase and defined as the time difference between the fAHP and the most depolarized voltage in a 200-ms window.

Maximal firing frequency (Fmax, AP/s): maximal firing frequency evoked with 1-s-long depolarizing current steps.

Only cells with a resting membrane potential more negative than −50 mV were included for analysis of current clamp experiments. Series resistance was maintained below 40 MΩ throughout the recordings.

2.5 | Histology

Mice used for histological analysis were anaesthetized with isoflurane and then euthanized with an overdose of pentobarbital (i.p. 100 mg/kg, Apotekerforeninger). The mice were intracardially perfused with Ringer solution (.85% NaCl, .025% KCl, .02% NaHCO3) followed by 4% paraformaldehyde (PFA) in phosphate buffer (PB) (pH 7.4). The brain was extracted from the skull and

placed in 4% PFA for 3 h before moving it to a solution containing 15% sucrose in PB overnight. The brains were then stored in 30% sucrose for 2 days before being sliced at 50 μm with a freezing microtome. Slices were collected in six equally spaced series and placed in tubes containing a solution composed of 30% glycerol, 30% ethylene glycol and 40% phosphate buffer saline (PBS). The tissue was stored at −20°C until used for histology.

The slices were washed in PB (3 × 10 min) before incubation with blocking solution (.1% Triton-X, 10% NGS in PB). After blocking, the tissue was incubated with the primary antibody for 3 days at 4°C in a solution containing: .1% Triton-X, 1% NGS in PB. After being washed (3 × 1 h in PB), the tissue was incubated with the secondary antibody overnight at 4°C. The slices were washed (3 × 10 min in PB) and mounted on SuperFrost slides (Termo Fisher Scientific) and left to dry overnight. The slides were coversliped with entellan xylene (Merck Chemicals, Darmstadt, Germany) after being washed in xylene for 15 min or with Fluoromount after being washed in distilled water for about 30 s. We used the following primary antibodies: Guinea Pig IgG anti-NeuN (1:1000, Sigma Millipore, #ABN90P), Rabbit anti-PV (1:1000, Swant, #PV-27), Mouse IgG1 anti-PV (1:1000, Sigma, #P3088), Rat IgG2a anti-RFP (1:1000, Proteintech, #5f8), Chicken IgY anti-GFP (1:1000, Abcam, #ab13970), Rabbit IgG anti-SST (1:1000, BMA Biomedicals). We used the following secondary antibodies: Goat anti-guinea pig (IgG H + L) A647 (1:500, Invitrogen, #A-21450), Goat anti-Rat (IgG H + L) A-546 (1:500, Invitrogen, #A11081), Goat anti-Rabbit (IgG H + L) A488 (1:500, Invitrogen, #A11008), Goat anti-chicken (IgY H + L) A488 (1:500, Invitrogen, #A11039), Goat anti-rabbit (IgG H + L) A546 (1:500, Invitrogen, #A11010), Goat anti-rabbit (IgG H + L) A635 (1:500, Invitrogen, A31576).

2.6 | Image acquisition and analysis

We used a confocal microscope (Zeiss LSM 880 AxioImager Z2) to image regions of interest (ROIs) to count labelled neurons. We imaged ROIs including the following cortical areas: 3 slices/mouse primary somatosensory cortex whisker field (wS1), 2 slices/mouse primary visual cortex (V1), 3–5 slices/mouse perirhinal cortex (PER), 3–5 slices/mouse ectorhinal cortex (ECT), 2 slices/mouse prelimbic cortex (PrL) and 2 slices/mouse infralimbic cortex (IL). Images of ROIs were taken with a ×20 air objective (.8 NA) with pinhole size of 1 Airy unit throughout the 50-μm thickness of the slices and saved as czi files. We selected 2–5 ROIs for each cortical region. ROIs contained the whole cortical area of interest in a given slice. Files containing the ROIs were uploaded in Neurolucida360 (Micro Bright Field Bioscience) for analysis. We manually created contours to delineate the layers of the ROIs using the PV signal: layer 4 in sensory areas was identified as the layer with the densest staining bordered by layer 2/3 superficially and layer 5A as a layer with low density of PV staining. PER and ECT were delineated according to Beaudin et al. (2013). We use here the nomenclature of PER (perirhinal) and ECT (ectorhinal) as reported in the Allen Brain Atlas and in the Franklin and Paxinos (2007) atlas. These two cortical regions correspond to A35 and A36 of the nomenclature used in Beaudin et al. (2013) and in several other reports on different rodent and primate species. We opted to follow the nomenclature of the Allen Brain Atlas to allow for easier comparison with previous quantifications of inhibitory cell types in the cortex (Kim et al., 2017; Whissell et al., 2015). PrL and IL were delineated according to Van De Werd et al. (2010). These delineations agreed with cytoarchitectural features obtained from the NeuN signal from adjacent slices. Symbols for each fluorescent signal were used to manually count cells labelled by different markers. We counted all cells contained within the contours. A cell was counted if its soma was completely inside a contour. Markers were manually applied onto the section of the confocal stack containing the center of the cell soma. For the quantification of GABA and SST neurons, we used the overlap with NeuN to make sure the signal was indicative of a neuron. This was deemed necessary because of the immunostaining pattern for these antigens that label the soma but not the dendrites. Because we counted slices distanced 300 μm from each other, overcounting in the z axis is not relevant, and we did not apply any correction. Quantification of the number of markers in each contour was done in Neurolucida Explorer (Micro Bright Field Bioscience) and exported in Microsoft Excel. The density of neurons labelled by a marker was measured as the number of labelled neurons in a contour divided by the area of the contour (cells/mm^2). The GAD67-GFP mouse line was previously described as labelling all neocortical GABAergic neurons, including PV, SST and calretinin expressing neurons (Tamamaki et al., 2003). We performed immunofluorescence for GABA in two mice and quantified the efficiency of the mouse line in targeting GABAergic neurons in PER/ECT region. We chose the PER/ECT region because we have previously shown that in this area, the PV-cre mouse line was not efficient (Nigro et al., 2021). The two mice showed a very high overlap between GABA and GFP (mouse 1: 94.14%; mouse 2: 92.23%) (Figure S1, Data S1). The GAD67-GFP mouse line labelled virtually all PV-INs but showed a lower specificity for SST-INs across all cortical areas included in our study (Figure 1a–p; Table 1; Dataset S2). For this reason, the

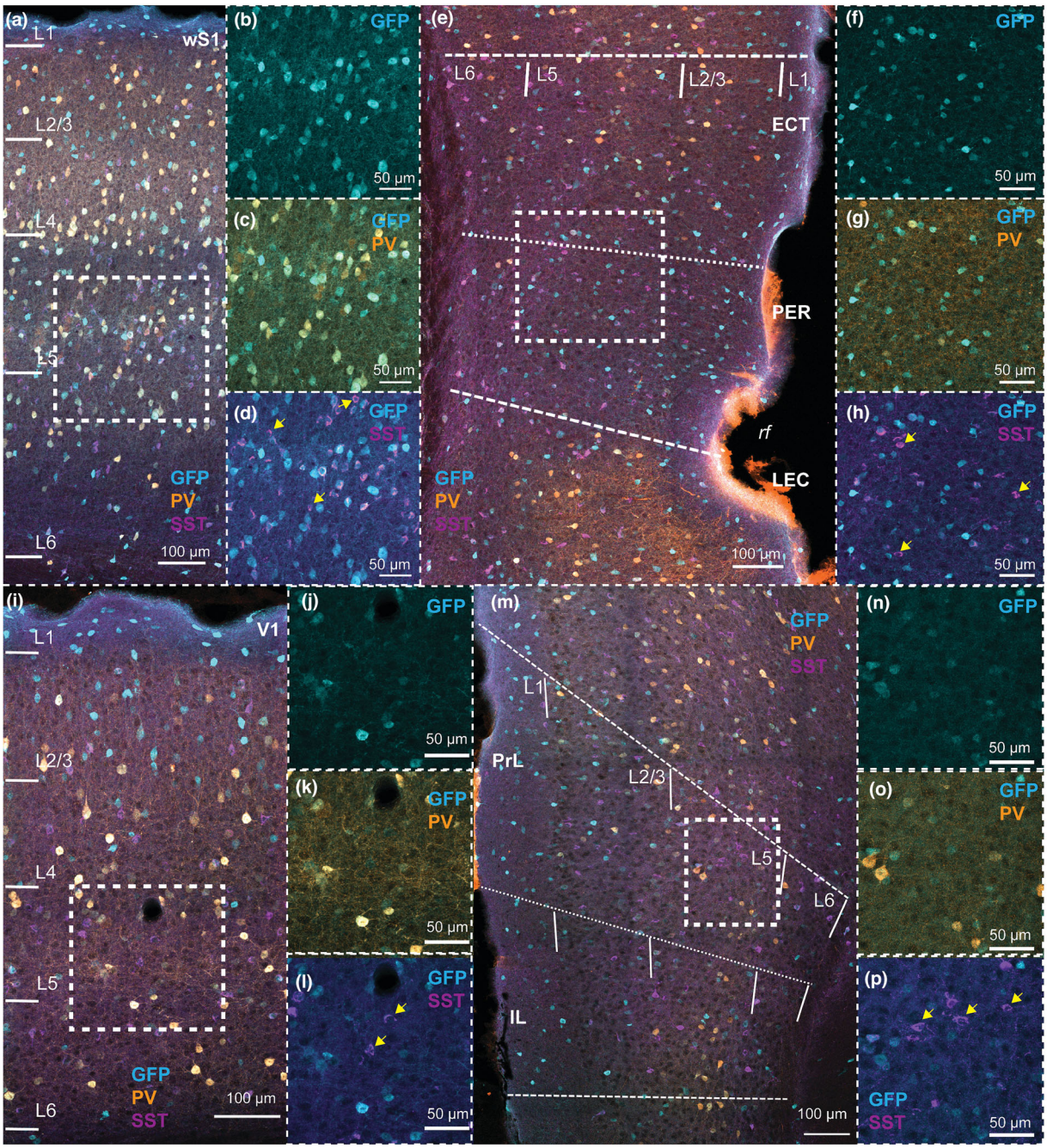

FIGURE 1 Efficiency of the GAD67-GFP mouse line to label parvalbumin (PV) and somatostatin (SST) neurons. (a) Representative confocal stack of a section of wS1 showing the overlap of the signals for GFP (turquoise), PV (orange) and SST (violet). (b–d) Magnified pictures of the area enclosed in the white square in a showing the signals for green fluorescent protein (GFP) (b), GFP and PV (c) and GFP and SST (d). Arrows in d point at cells expressing SST but not GFP. (e–h) Same as in a–d but for PER/ECT. h shows that also in PER/ECT, some SST neurons are not labelled by GFP (arrows). LEC, lateral entorhinal cortex; rf, rhinal fissure. (i–l) Same as for a–d but for V1. l shows that also in V1, some SST neurons do not express GFP (arrows). (m–p) Same as for a–d but for PrL/IL. p shows that in PrL/IL, some SST neurons do not express GFP.

number of PV-INs and SST-INs were measured from the immunolabelling for the specific marker, independently of GFP expression. Transcriptomic analysis of the neuronal population of the cortex shows that SST and PV are expressed exclusively in GABAergic neurons (Tasic et al., 2016). We excluded from the counting a small population of PV-IR pyramidal neurons in L5B of wS1 (van Brederode et al., 1991). Values are reported as mean ± standard deviation. All graphs were created in Microsoft Excel or Matlab 2021a (Mathworks); images of ROIs were created in Zen lite (Zeiss) and figures in Adobe Illustrator.

TABLE 1 Efficiency of the GAD67 mouse line to label SST-INs and PV-INs in the six cortical areas included in this study. Rows represent the layers in each cortical area. Values in columns represent the mean and standard deviation (in parentheses) of the number of SST-INs, PV-INs and the efficiency for each. The mouse line consistently showed a slightly lower efficiency for SST-INs.

Layer/ cortex	SST (cells) ($n = 3$ mice)	SST/GFP+ (cells) ($n = 3$ mice)	Efficiency (%) ($n = 3$ mice)	PV (cells) ($n = 3$ mice)	PV/GFP+ (cells) ($n = 3$ mice)	Efficiency (%) ($n = 3$ mice)
L1/V1	3 (0)	2 (1)	66.7 (33.3)	1.7 (2.1)	.3 (.6)	12.5 (17.7)
L2/3/ V1	58 (2.7)	52 (2)	89.9 (6.9)	118.7 (7.2)	117.3 (7.6)	98.9 (.5)
L4/V1	78.7 (18.5)	66 (18.1)	83.6 (9.9)	128.7 (31.8)	128.3 (32.3)	99.6 (.6)
L5/V1	142.7 (37.2)	118 (36.5)	82.5 (9.6)	194 (44.9)	193 (43.3)	99.6 (.7)
L6/V1	94.67 (24.03)	74 (22.9)	77.9 (9)	115.7 (31.4)	115.6 (31.4)	100 (0)
L1/wS1	2 (2.6)	2 (2.7)	100 (0)	0 (0)	0 (0)	
L2/3/ wS1	56 (7.2)	42.3 (1.5)	76.2 (7.6)	113.3 (10.5)	112 (10)	98.8 (.4)
L4/wS1	68 (4.4)	45.3 (7.5)	67.3 (15.5)	221 (42.6)	220.7 (42.0)	99.9 (.2)
L5/wS1	142.7 (32)	119.7 (25.4)	84.0 (3.6)	234.3 (42.2)	234.3 (42.2)	100 (0)
L6/wS1	118.3 (19.6)	85 (6.2)	72.6 (6.9)	144.7 (14.6)	144.3 (14.0)	99.8 (.4)
L1/A36	2.7 (2.3)	2.7 (2.3)	100 (0)	.7 (.6)	.3 (.6)	100 (0)
L2/3/ A36	72.3 (5.8)	60.3 (11.7)	83.8 (8.7)	46 (19.9)	45.3 (20.5)	99.6 (2.4)
L5/A36	137 (26.1)	106 (37.0)	78.8 (8.8)	103.7 (34.5)	102.7 (35.1)	99.0 (2)
L6/A36	56.3 (7.1)	49.7 (8.1)	89.3 (4.7)	43.7 (6.0)	43.3 (6.5)	100 (0)
L1/A35	2.7 (.6)	2.7 (.6)	100 (0)	.3 (.7)	.3 (.6)	100 (0)
L2/3/ A35	74.7 (14.6)	60 (16.1)	80.9 (7.9)	23.3 (13.7)	22.7 (14.2)	99.8 (.4)
L5/A35	93.7 (15.9)	73.3 (12.0)	78.3 (5.6)	55.3 (32.9)	55.3 (32.9)	98.8 (2.4)
L6/A35	51.7 (5.5)	44.7 (3.8)	89.6 (4.3)	26 (14)	26 (14)	100 (0)
L1/PrL	7.7 (4.0)	5.3 (3.2)	69.0 (10.3)	1.7 (.6)	1.3 (.6)	83.3 (28.7)
L2/3/ PrL	50 (8.2)	29.3 (9.1)	58 (12.6)	19 (5.3)	18.3 (5.1)	96.4 (3.4)
L5/PrL	129 (12.1)	64.3 (31.6)	49.1 (20.3)	97.3 (14.3)	95 (15.7)	97.4 (1.9)
L6/PrL	49.7 (4.0)	27.3 (9.1)	54.3 (13.6)	20.7 (6.0)	19.7 (4.5)	96.3 (6.4)
L1/IL	1 (0)	.7 (.6)	66.7 (57.7)	1 (1)	1 (1)	100 (0)
L2/3/IL	21 (9.8)	13.3 (5.5)	66.2 (16.3)	3.7 (1.5)	3.3 (1.5)	91.7 (14.4)
L5/IL	77 (12.3)	41.3 (26.3)	51.1 (24.3)	61.7 (13.6)	60 (12.8)	97.5 (2.5)
L6/IL	47.7 (10.2)	31.3 (13.1)	64.1 (15.5)	21 (7.2)	20.3 (7.0)	97.1 (5.0)

Abbreviations: GFP, green fluorescent protein; PV, parvalbumin; SST, somatostatin.

2.7 | Statistics

Principal component analysis on the densities of different GABAergic neurons across layers of PER and wS1 was performed in Matlab 2021 (Mathworks) using the function 'pca'. We obtained the explained variance for each principal component, the principal component coefficients, the principal component scores and the principal component variances. Hierarchical cluster analysis was performed in Matlab 2021 (Mathworks). After normalization with the function 'zscore', we calculated the distance between pairs of objects with the function 'pdist' and the method 'cityblock'. Objects were grouped according to the calculated distances with the function 'linkage' and the method 'average'. After calculating the inconsistency index ('inconsistent'), clusters were obtained by using the function 'cluster' and the inconsistency index as cutoff. This method identified two clusters.

We assessed statistical significance of differences in cell density using slices as samples ($n = 6$ for V1, PrL and

IL; $n = 9$ for wS1; $n = 15$ for PER and ECT). Statistical significance was tested with one-way analysis of variance (ANOVA) (6 groups) followed by Bonferroni correction for multiple comparisons ($\alpha = 0.0033$).

We did not use any statistical method to predetermine sample size. The number of mice, slices or neurons used are consistent with other studies in the field (Kim et al., 2017; Ma et al., 2006; Nigro et al., 2018; Whissell et al., 2015). No blinding method was used. When appropriate, statistical comparison was performed with a one-way ANOVA with Bonferroni correction for comparing more than two groups, or with a two-sided Wilcoxon rank sum test for comparing two groups.

3 | RESULTS

3.1 | Comparison of the GABAergic population of primary sensory and association areas

Previous brain-wide quantifications of cortical GABAergic neurons highlighted a prominent drop in density of PV-INs in association areas (Kim et al., 2017; Whissell et al., 2015). The interpretation of the results of these studies rests on the assumption that the mouse lines used for quantifying PV-INs reflect the intrinsic expression pattern of PV throughout the cortex (Kim et al., 2017; Whissell et al., 2015). Previous quantifications of labelled neurons in the PV-cre mouse line led to the conclusion that association areas are under a lower inhibitory control because of the low density of PV-INs (Ding et al., 2024; Kim et al., 2017; Whissell et al., 2015). However, the total GABAergic population has not yet been quantified, and other GABAergic types might take on the role of PV-INs in association areas. We have previously described that the PV-cre mouse line is not efficient in association areas (PER, ECT, LEC, PrL, IL) and captures only 50% of PV-INs (Nigro et al., 2021). To test whether the density of PV-INs is in fact lower in association areas and to quantify the total GABAergic population in these regions, we used the GAD67-GFP mouse line ($n = 3$) and performed immunofluorescence staining for PV, SST and GFP (Figures 1 and 2). We found that the pattern of density distribution across cortical areas was still present when quantifying PV expression by immunofluorescence (Figure 2a–c). PV-INs were more abundant in the dorsal sensory and motor cortices as compared with medial associative (PrL and IL) and ventro-lateral associative areas (ECT and PER) (Figure 2a–c). We quantified the number of PV-INs, SST-INs and GFP-only neurons (neurons labelled by the GAD67-GFP mouse line but not expressing either PV or SST) across layers of six cortical areas (wS1, V1, PER, ECT, PrL, IL) and calculated their densities. We performed a PCA on the densities of these markers across the layers of these six areas to visualize in low dimensional space how these cell-types describe these six cortical regions (Figure 3a,b). The first two principal components accounted for 85.7% of the variance, and the data were well segregated in the principal component space (Figure 3a). Indeed, sensory cortices were grouped on the left side of the plot, pushed there by the higher density of PV-INs in these areas. On the other hand, association areas were spread along the horizontal axis in the right side of the PC space. The variables that best explained the variance were the density of PV-INs in layers 2/3 and 5, which was higher in sensory areas, and the density of GFP-only neurons in layers 2/3–6, which was higher in association areas (Figure 3b).

The pattern of distribution of the density of marker-expressing neurons across the six cortical areas was in agreement with previous quantifications (Kim et al., 2017; Whissell et al., 2015) (Figure 3c). However, the density of total GABAergic neurons was comparable across all regions (Figure 3c), and only wS1 had a significantly lower density of GABAergic neurons as compared with V1 and the rhinal cortices (one-way ANOVA, $p = 1.05\text{E}^{-9}$; Bonferroni, wS1 vs. V1: $p = 0.0024$; wS1 vs. ECT: $p = 1.48\text{E}^{-5}$; wS1 vs. PER: $p = 8.4\text{E}^{-6}$). Interestingly, the density of GFP-only neurons increased in association areas (one-way ANOVA, $p = 1.73\text{E-}^{17}$), with a trend that was specular to the reduction of PV-INs in these cortices (Figure 3c). The density of GFP-only neurons in the two sensory cortices was not statistically significantly different (Bonferroni, wS1 vs. V1: $p = 0.038$). The density of GFP-only neurons was significantly different between the sensory areas and the PER/ECT region (Bonferroni, wS1 vs. ECT: $p = 8.67\text{E-}^{11}$; wS1 vs. PER: $p = 2.36\text{E}^{-12}$; V1 vs. ECT: $p = 1.69\text{E}^{-8}$; V1 vs. PER: $p = 5.23\text{E}^{-10}$). Medial prefrontal areas (PrL/IL) were not significantly different than V1, but the density of GFP-only neurons was significantly different between wS1 and IL (Bonferroni, $p = 0.002$). Among association areas, the density of GFP-only neurons was significantly higher in rhinal cortices than in medial prefrontal areas (Bonferroni, ECT vs. PrL: $p = 0.0003$; ECT vs. IL: $p = 0.0018$; PER vs. PrL: $p = 3.4\text{E}^{-5}$; PER vs. IL: $p = 0.0001$). No significant difference was found between association cortices of the same network (rhinal or medial prefrontal). These data suggest that a higher density of GABAergic neurons that do not express either PV or SST compensates for the reduction in PV-INs in association cortices. We found similar patterns when comparing individual layers across cortical areas (Figure 3d–f).

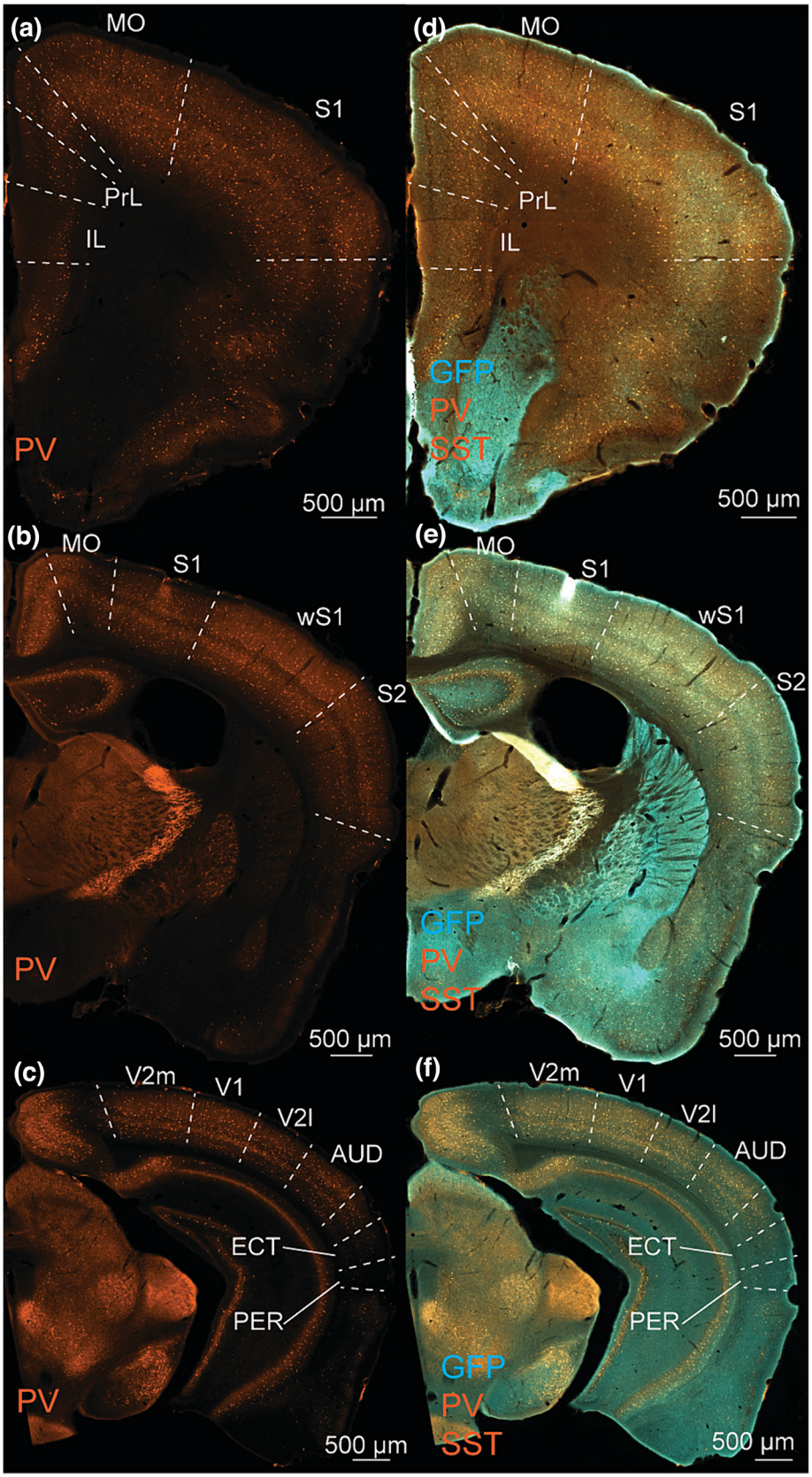

FIGURE 2 Gradients of parvalbumin (PV) expression along the rostro-caudal and dorso-ventral axes of the mouse brain. (a–c) Representative images of a staining for PV in a GAD67-GFP mouse along the rostro-caudal axis encompassing all cortical areas included in this study. Pictures from a to c show different slices along the rostro-caudal axis. (a) The intensity of PV staining drops in PrL/IL as compared to motor (MO) and sensory areas (S1). Proceeding caudally, the intensity of PV staining drops in lateral and ventral cortical areas (ventral to S2 in b) and at the level of PER/ECT in c. (d–f) Same slices as in a–c but showing the signal for green fluorescent protein (GFP, turquoise) and both somatostatin (SST) and PV (orange). Note how the GFP signal becomes more evident in the areas with low PV.

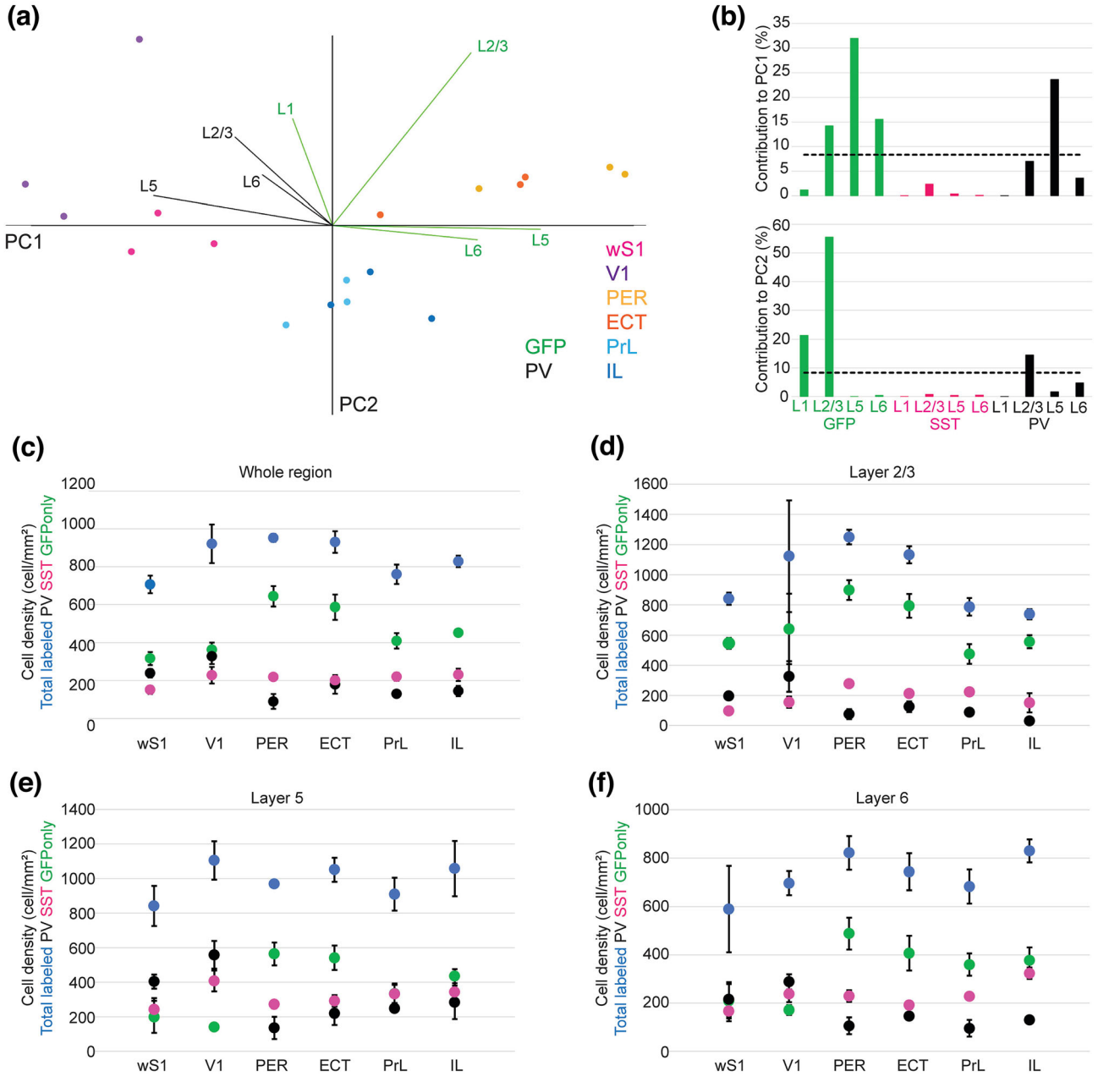

FIGURE 3 Density distribution of molecularly defined GABAergic types across six cortical areas. (a) Data from 3 mice were plotted in principal component space using the first two principal components. Data points are colour coded for cortical area, and each area contains three data points representing each mouse. Vectors represent the direction and weight (length of the vector) of the variables that mostly contribute to each principal component. Vectors are colour coded for cortical layer and molecular type. (b) Bar plots showing the contribution to the variance of the population by each variable (density of molecular type in each layer) for PC1 (upper panel) and PC2 (lower panel). The dotted line shows the level at which all variables would have equal contribution. (c–f) Plots of density of molecularly defined GABAergic neurons across cortical regions ($n = 3$ mice in each region). Data points are colour coded for molecular type. (c) Cell densities in whole cortical areas (i.e., combining all layers together). (d–f) Cell densities across areas in layer 2/3 (d), layer 5 (e) and layer 6 (f). See text for statistical comparisons.

3.2 | Electrophysiological census of the GABAergic population in wS1 and PER

Our histological examination demonstrates that although the density of PV-INs in association areas is lower than in sensory cortices, the density of GABAergic neurons is comparable. This suggests that some other GABAergic neurons might account for the increased density of GFP-only neurons. Some molecular classes of GABAergic neurons show specific biophysical properties that endow

them with specific firing patterns. Indeed, PV-INs are mostly fast-spiking, whereas SST neurons are mostly adapting or low-threshold spiking (Tremblay et al., 2016). We performed an electrophysiological examination of the firing properties of GFP-expressing neurons in the GAD67-GFP mouse line ($n = 18$) in layer 5 of wS1 and PER (Dataset S3). We chose layer 5 of wS1 because its GABAergic population has been extensively characterized and contains the highest density of PV-INs in wS1. We chose layer 5 of PER because it shows the lowest density of PV-INs across association cortices. We reasoned that this comparison would maximize our chances to identify the firing pattern of the GABAergic population not expressing PV.

Unexpectedly, the fast-spiking phenotype accounted for the largest population in both PER and wS1 (Figure 4a), which is at odds with the low density of PV-INs in PER (Figure 2). Interestingly, the proportion of fast-spiking cells was comparable in wS1 (55%) and PER (52%) (Figure 4a) and much higher than expected from the histological examination of PV expression (Figure 4b). Fast-spiking neurons in PER had local axon and dendrites, similar to local fast-spiking neurons in wS1 (Figure 4c). We hypothesized that some fast-spiking neurons in PER do not express detectable levels of PV. To test this hypothesis, we labelled fast-spiking neurons with a viral approach that exploits enhancer driven expression of tdTomato in fast-spiking INs throughout the brain

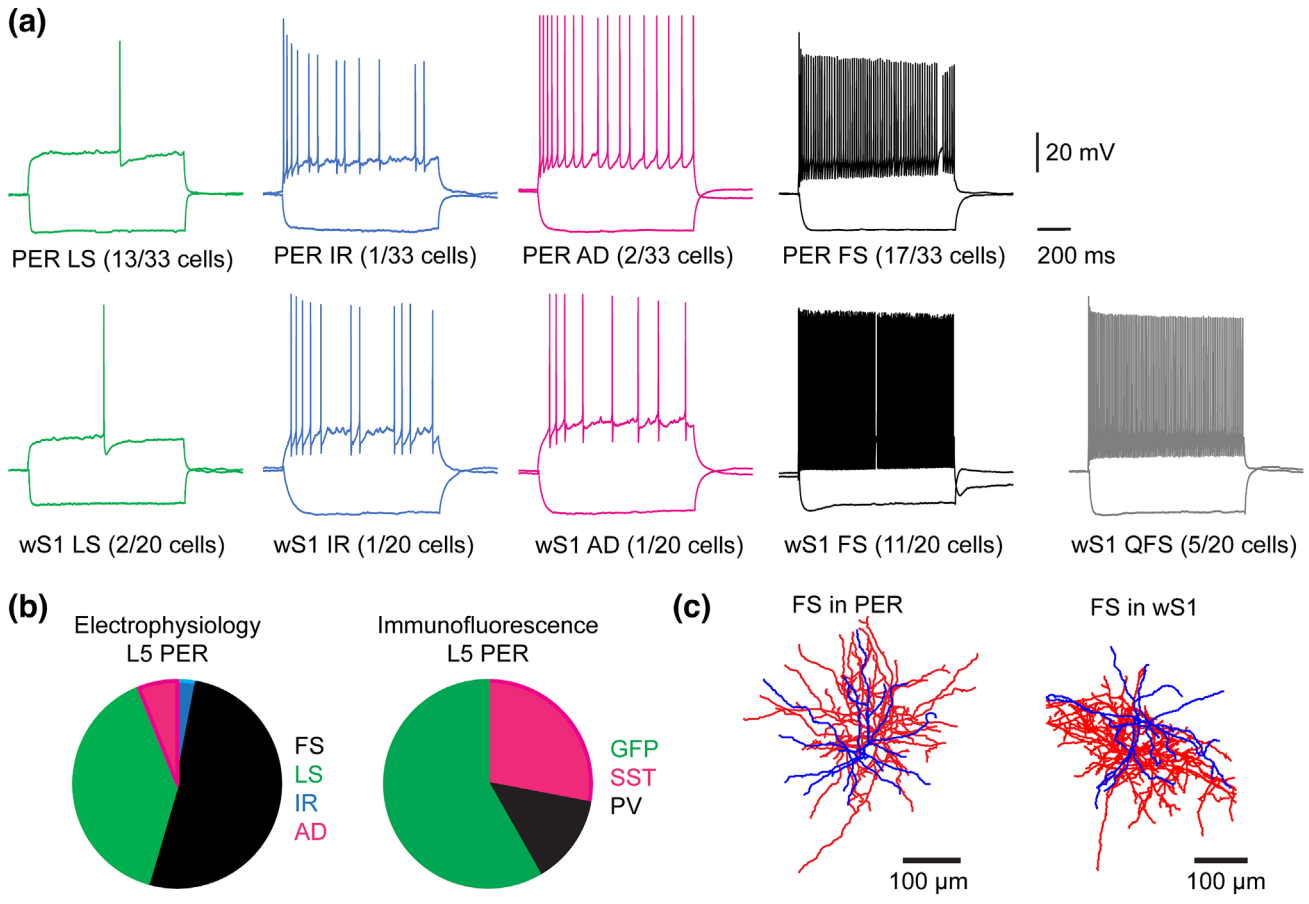

FIGURE 4 Electrophysiological census of GABAergic types in layer 5 of wS1 and perirhinal cortex (PER) in the GAD67-GFP mouse line. (a) Representative voltage responses to hyper- and depolarizing current injections colour coded for pattern type in PER (upper row) and wS1 (lower row). Green, late-spiking pattern characterized by a long latency to first spike near rheobase, broad AP_{HW}, broad afterhyperpolarization (AHP) and absence of sag; blue, irregular spiking pattern characterized by early adaptation followed by spiking at irregular intervals; red, adapting firing pattern characterized by adaptation of firing frequency followed by regular spiking; black, fast-spiking pattern characterized by the highest maximal firing frequency, low input resistance, short AP_{HW} and fast AHP; grey, quasi-fast spiking pattern (only in wS1), similar to the fast spiking but with higher input resistance (IR), lower firing rates and stronger adaptation (see Ma et al., 2006; Nigro et al., 2018). (b) Pie charts comparing the percentages of different firing patterns (left) and molecular types (right) in layer 5 of PER. Colour codes follow the one used for firing pattern in a and assumes the equivalence of the fast-spiking pattern with parvalbumin (PV)-INs. (c) Representative recovered morphologies of fast-spiking neurons in PER (left) and wS1 (right). Dendrites are coloured in blue and axons in red.

(Vormstein-Schneider et al., 2020). This approach does not lean on the expression of PV in FS neurons, but the enhancer has been shown to be associated to the expression of the Nav1.1 channel (Vormstein-Schneider et al., 2020). We injected the S5E2-dTom virus in PER/ECT of C57 mice ($n = 6$) and characterized the electrophysiological properties of the cells labelled by the S5E2-tdTom virus (Figure 5a,b). Most labelled neurons showed a fast-spiking phenotype (16/18), characterized by low input resistance, short AP duration and high maximal firing frequency with minimal adaptation (Figure 5b). We found 2 (out of 18) neurons that showed adapting ($n = 1$) and LTS ($n = 1$) firing patterns (Figure 5b). These firing patterns are characteristic of SST-INs as demonstrated by recordings performed in PER of SST-cre mice ($n = 3$ mice) (Figure 5b).

To directly test the hypothesis that some fast-spiking neurons in PER do not express PV, we performed immunofluorescence for PV on 15 of the recorded fast-spiking neurons and found that 6 out of 15 did not show detectable levels of PV (E2-PV-) either in their soma or axons (Figure 5c–j; Figure S2). A comparison of the electrophysiological properties of PV-IN and E2-PV- revealed that the two populations have similar biophysical properties despite the difference in PV expression (Table 2). Interestingly, when comparing fast-spiking neurons in PER and wS1, we found several electrophysiological differences, with fast-spiking neurons in wS1 having faster HW and AHPs, which enables them to reach a higher maximal firing frequency (Figure 6b–g). We used hierarchical clustering on the electrophysiological parameters and further confirmed the difference between fast-

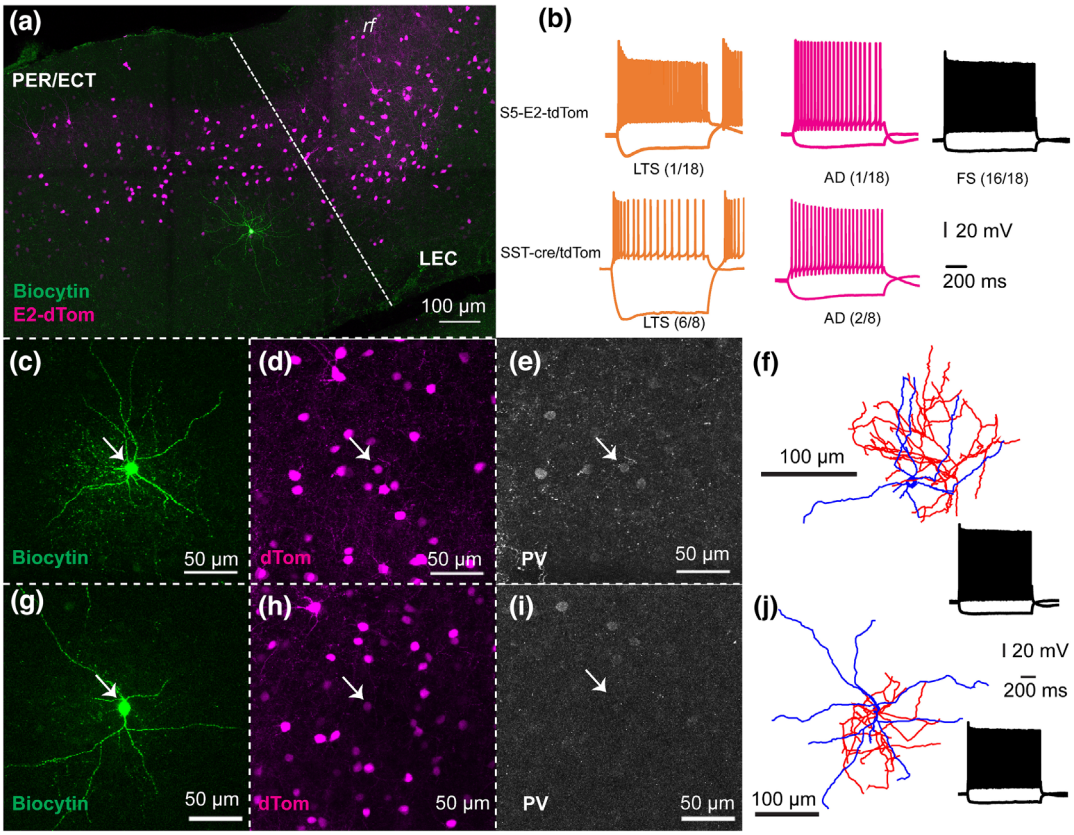

FIGURE 5 Electrophysiological characterization of neurons labelled by the S5E2-dTom virus in layer 5 of perirhinal cortex (PER) of C57 mice. (a) Representative image of a brain slice containing PER from a C57 mouse injected with the S5E2-dTom virus. Neurons labelled by the virus are shown in magenta and the recorded neuron in green. LEC, lateral entorhinal cortex; rf, rhinal fissure. (b) Representative voltage responses to hyper- and depolarizing current injections of neurons recorded from C57 mice injected with the S5E2-dTom virus (upper row) and in the PER of somatostatin (SST)-cre/tdTom mice. Voltage responses are colour coded for firing patterns: orange, low-threshold spiking characterized by high input resistance, low threshold for antero-posterior (AP) generation and rebound bursting (Ma et al., 2006; Nigro et al., 2018); red, adapting firing pattern; black, fast-spiking pattern. (c–e) Example neurons showing the expression of PV in fast-spiking neurons labelled by the S5E2-dTom virus in PER. (f) Recovered morphology and firing pattern of the cell in c. Dendrites are coloured in blue and axons in red. (g–i) Lack of PV expression in an example fast-spiking neuron labelled by the S5E2-dTom virus in PER. (j) Recovered morphology and firing pattern of the neuron in g.

TABLE 2 Electrophysiological properties of fast-spiking cell expressing PV and not expressing PV in layer 5 of PER. Cells were labelled with the S5E2-dTom virus injected in C57 mice. Values report the mean and standard deviation (in parentheses). The last row reports the *p* value of a Wilcoxon rank sum test.

	IR (MΩ)	Sag	Rheobase (pA)	AP_{thr} (mV)	AP_{hw} (ms)	fAHP (mV)	AHP_{dur} (ms)	F_{max} (AP/s)	I_{block} (pA)
PV + ($n = 9$)	310.2 (82.4)	.94 (.02)	103.3 (44.5)	−19.5 (2.4)	.43 (.07)	24.4 (5.7)	53.6 (15.9)	116.6 (29.1)	442.0 (79.8)
PV – ($n = 6$)	272.8 (63.9)	.94 (.01)	111.3 (31.6)	−21.0 (1.1)	.42 (.08)	22.7 (1.6)	56.9 (25.8)	107.5 35.8	403.4 (72.8)
p	0.69	1	0.39	0.09	0.78	0.95	0.95	0.46	0.33

Abbreviations: AHP, afterhyperpolarization; AP, antero-posterior; IR, input resistance; PER, perirhinal cortex; PV, parvalbumin; SST, somatostatin.

spiking neurons in the two cortical areas (Figure 6a). In PER, PV-INs and E2-PV- were clustered together, further confirming that their electrophysiological properties are indistinguishable (Figure 6a).

Our electrophysiological characterization of GABAergic neurons demonstrates that PER contains a large population of fast-spiking neurons that do not express detectable levels of PV and are not labelled by the PV-cre mouse line. However, these neurons can be labelled by an enhancer-driven viral strategy that is independent from the expression of PV. Does this population of fast-spiking neurons not expressing PV account for the increased proportion of GABAergic neurons not expressing PV or SST in association cortices?

3.3 | Association cortices contain fast-spiking INs that do not express PV

The experiments described above demonstrate that PER contains a large number of fast-spiking GABAergic neurons that do not express PV and that has been so far unacknowledged by previous estimations of GABAergic types across cortical areas (Kim et al., 2017; Whissell et al., 2015). To test whether this population is also present in other association areas, we developed an intersectional viral approach to specifically label fast-spiking GABAergic neurons while excluding SST-INs (Figure 7). As demonstrated by our electrophysiological characterization of the E2-dTom labelled neurons, we found that SST-INs account for about 20% of the labelled neurons in PER/ECT of GAD67-GFP mice ($n = 2$) (Figure 7a–c). To exclude the SST-INs, we inserted lox sites for the cre-dependent excision of the tdTomato sequence and additional lox sites for the cre-dependent inversion of an inverted sequence coding for GFP (Figure 7d). When injected in PER/ECT of an SST-cre mouse, this strategy labelled E2/SST-INs with GFP and E2/SST- fast-spiking neurons with tdTomato (Figure 7e–g; Dataset S4). We found virtually no overlap between E2-dTom and E2-GFP neurons (Figure 7f) and virtually all E2-GFP neurons expressed SST (Figure 7g). To test whether fast-spiking neurons not expressing PV are present in other association areas, we injected the intersectional virus in PER/ECT and PrL/IL cortex of SST-cre mice ($n = 2$) (Figure 8a,b). In PER/ECT, only about 40% of putative fast-spiking neurons express PV, and about 65% of putative fast-spiking neurons in PrL/IL express PV, suggesting that a large population of fast-spiking neurons in association cortices do not express PV (Figure 8c). These results further confirm our histological examination of the patched fast-spiking neurons not expressing PV and suggest that cytoplasmic dialysis due to whole-cell procedure might not be responsible for the lack of PV expression in our patched samples (Figure 5). We also quantified the density of tdTomato expressing neurons in PER/ECT and in PrL/IL areas and observed that it was comparable with the density of PV-INs in wS1 and V1 (one-way ANOVA, $p = 8.41E\text{-}10$; Bonferroni ($\alpha = 0.0033$), PER/ECT-E2 labelled vs. wS1-PV, $p = 0.048$; mPFC-E2 labelled vs. wS1-PV, $p = 0.96$; PER/ECT-E2 labelled vs. V1-PV, $p = 0.46$; mPFC-E2 labelled vs. V1-PV, $p = 0.11$) (Figure 8d). These results confirm our hypothesis that the population of fast-spiking neurons not expressing PV accounts for the reduced density of PV-INs previously reported in these areas (Kim et al., 2017; Whissell et al., 2015).

4 | DISCUSSION

The present study challenged recent findings showing that the density of fast-spiking neurons in association cortices is lower than that of sensory cortices (Kim et al., 2017; Whissell et al., 2015). We demonstrate that association cortices contain a comparable density of GABAergic neurons to sensory areas despite the low

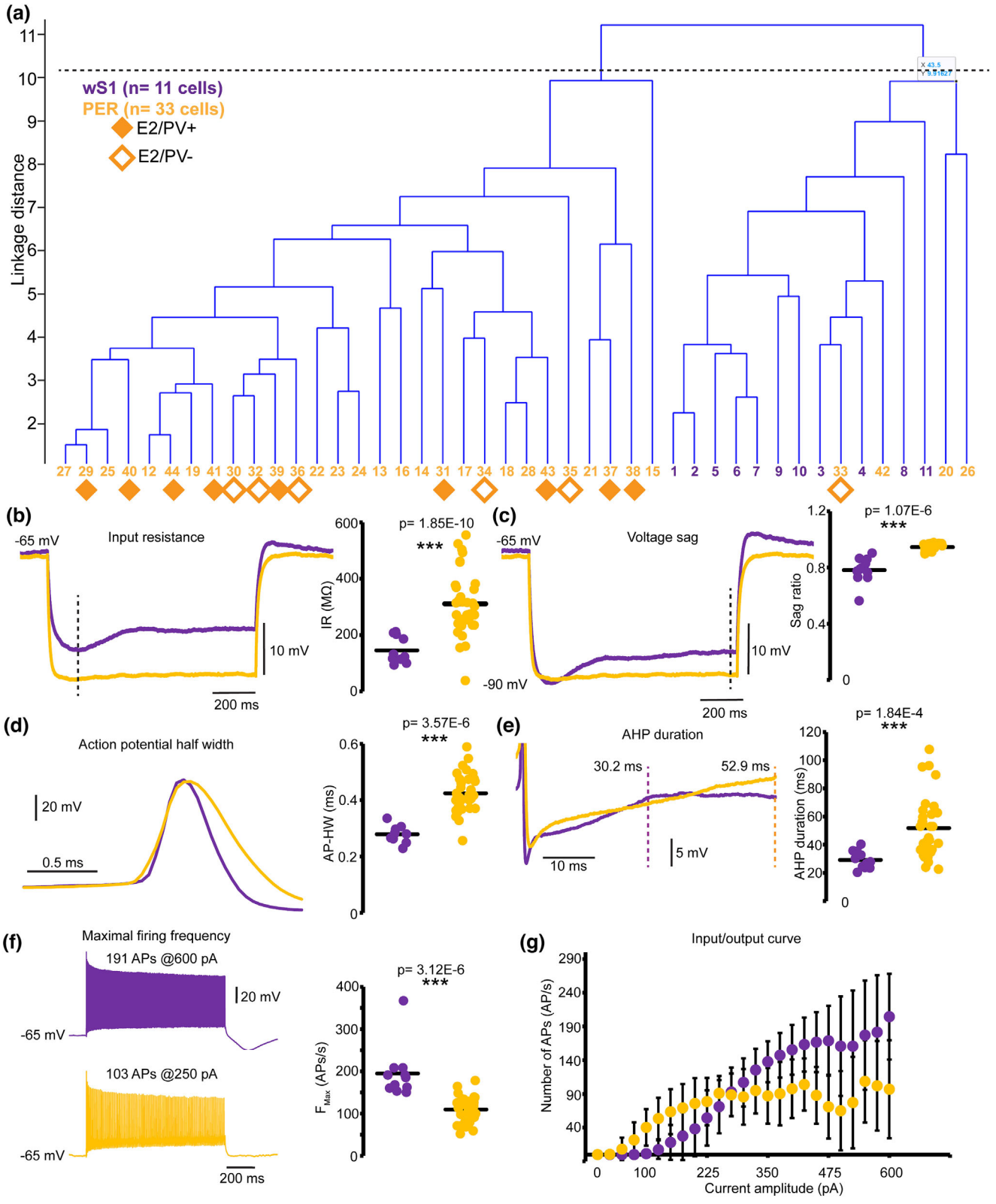

FIGURE 6 Legend on next page.

FIGURE 6 Fast-spiking neurons show region-specific electrophysiological properties independently of parvalbumin (PV) expression. (a) Dendrogram obtained by hierarchical cluster analysis of electrophysiological properties of neurons in wS1 and perirhinal cortex (PER). The cluster analysis revealed two clusters that largely overlap with the area of where neurons were recorded rather than with the expression of PV. (b–g) Comparison of the significantly different electrophysiological properties between wS1 (purple) and PER (yellow) neurons. Each panel shows representative voltage responses showing the indicated electrophysiological feature (left panel) and the plot of the distribution for all neurons in the two areas (right panel). See Methods for details on the measurements of each electrophysiological property. *p* values for a Wilcoxon rank sum test are shown for each plot.

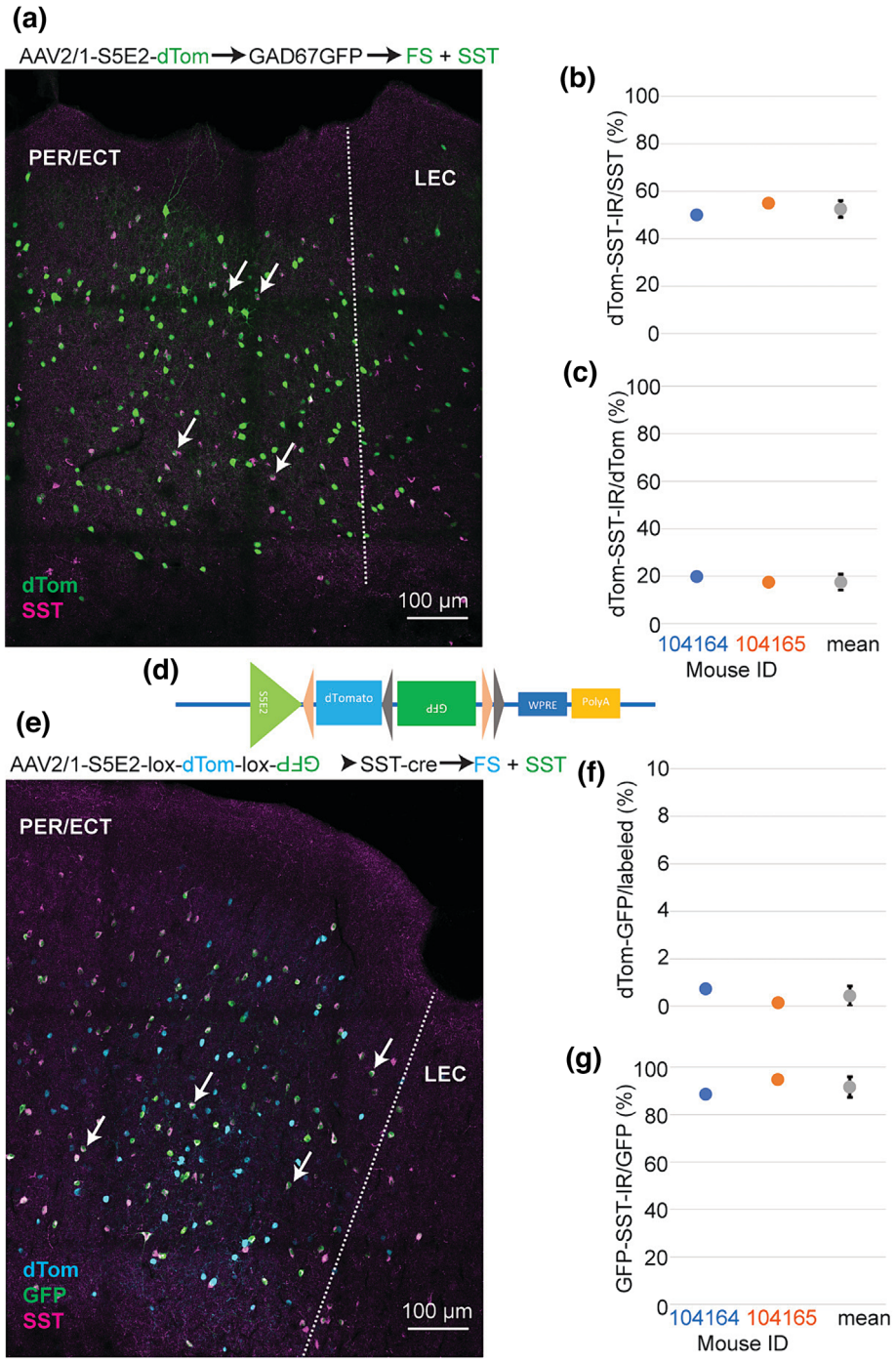

FIGURE 7 Intersectional viral strategy to label fast-spiking neurons while excluding somatostatin (SST)-INs. (a) Representative slice of perirhinal cortex/ectorhinal cortex (PER/ECT) of a GAD67-GFP mouse injected with the S5E2-dTom virus. Immunofluorescence for SST (magenta) and dTom (green) shows that some neurons labelled by the virus express SST (arrows). (b) Plot showing the percent of SST-INs labelled by the S5E2-dTom virus ($n = 2$ mice). (c) Plot showing the percent of neurons expressing dTom (labelled by the virus) that also express SST ($n = 2$ mice). (d) Schematics of the sequence of the intersectional virus. Pink triangles represent lox 2272 sites and grey triangles represent loxP sites. (e) Representative slice of PER/ECT of a SST-cre mouse injected with the intersectional virus. Immunofluorescence for dTom (turquoise), green fluorescent protein (GFP, green) and SST (magenta) shows no overlap between dTom and GFP expression and SST expression only in GFP labelled neurons (arrows). LEC, lateral entorhinal cortex. (f) Plot showing the percent of neurons expressing dTom and GFP in the population of labelled neurons (dTom + GFP) ($n = 2$ mice). (g) Plot showing that virtually, all GFP neurons express SST ($n = 2$ mice).

density of PV-INs. We provide multiple lines of evidence demonstrating that the fast-spiking population of association cortices is comparable with that of wS1, and a considerable number of these neurons do not express PV. We developed an intersectional viral strategy to label fast-spiking neurons that does not rely on PV expression

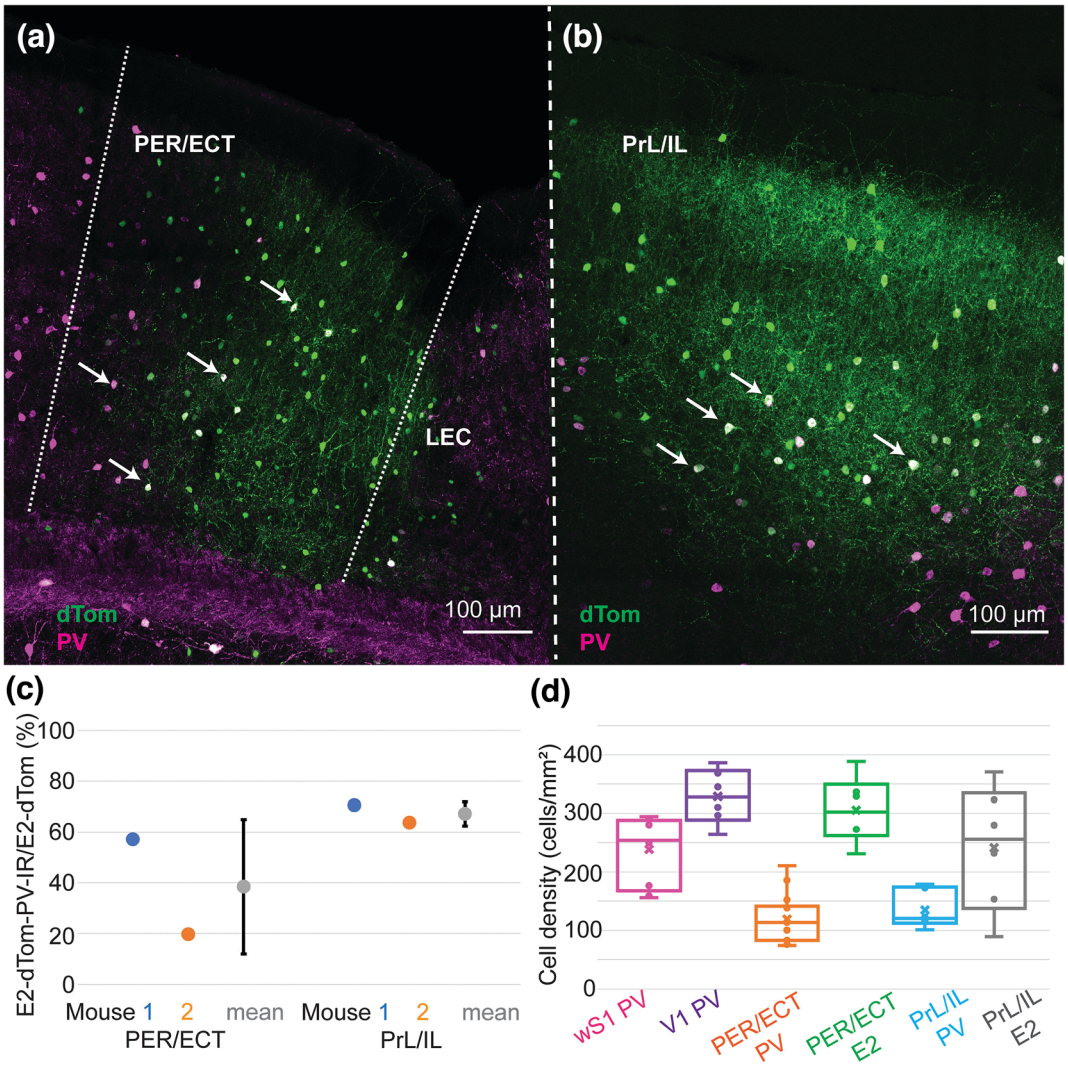

FIGURE 8 (a,b) Representative slices of PER/ECT (a) and PrL/IL (b) of somatostatin (SST)-cre mice injected with the intersectional virus. Immunofluorescence for parvalbumin (PV, magenta) revealed that some dTom (green) neurons do not express PV. Arrows indicate cells labelled by the virus and expressing PV. (c) Plot showing the percent of dTom expressing neurons that also express PV in perirhinal cortex/ectorhinal cortex (PER/ECT) and PrL/IL ($n = 2$ mice). (d) Bar plot comparing the density of putative fast-spiking neurons across cortical regions inferred from PV expression (first four columns, as in Figure 1c) and from the labelling by the intersectional virus (last two columns). See text for statistical comparison.

and demonstrate that a large population of fast-spiking neurons in association cortex does not express PV.

The low expression of PV in association cortices has been used by neuroanatomists to delineate these areas for several decades in different species (Beaudin et al., 2013; Burwell et al., 1995; Pitkänen & Amaral, 1993; Uva et al., 2004; Van De Werd et al., 2010). However, this observation has only recently been examined in the context of GABAergic cell-types and inhibitory circuits using specific mouse lines targeting PV-INs (Kim et al., 2017; Whissell et al., 2015). We have recently described that the labelling in the PV-Cre mouse line is very inefficient and quantifications of the number of PV-INs would be dramatically underestimated (Nigro et al., 2021). The present study corroborates the low density of PV-INs in PER/ECT by quantifying PV-INs neurons and extends this finding to PrL/IL areas. The fast-spiking population not expressing PV has been unacknowledged by previous quantifications of GABAergic neurons, likely because of the absence of a labelling tool, such as a molecular marker or mouse line.

We show that all fast-spiking neurons can be labelled by a viral strategy that is independent of PV expression and simultaneously excludes SST-INs. This further suggests that the two fast-spiking populations share other features related to gene expression, such as sodium channel subunit Nav1.1 and Kv3 potassium channels.

Interestingly, Taniguchi et al. (2013) described a large population of chandelier cells that was negative for PV in PFC (Taniguchi et al., 2013). The chandelier cells negative for PV might contribute to the fast-spiking population not expressing PV of association cortices. Indeed, a recent study shows that chandelier cells seem to be very abundant in PrL/IL and in PER/ECT areas, though their PV expression was not tested (Raudales et al., 2023). However, we did not find any electrophysiological difference in between PV-expressing and PV-negative fast-spiking neurons in PER, whereas Taniguchi et al. (2013) described several differences in the biophysical properties of chandelier cells as compared with PV-expressing basket cells (Taniguchi et al., 2013). Finally, visual inspection of the morphology of the recorded fast-spiking neurons in PER did not reveal any chandelier cells. This suggests that although chandelier cells are expected to contribute to the fast-spiking population we describe in association cortices, they cannot fully account for the fast-spiking population not expressing PV.

Our electrophysiological characterization demonstrates that fast-spiking INs show different biophysical properties in wS1 and PER. This might reflect specializations of biophysical properties related to computations performed in these two brain regions. In wS1 (and other primary sensory areas), PV-INs are involved in fast feedforward inhibition to constrain the integration window of excitatory postsynaptic potentials (Tremblay et al., 2016). Previous studies have shown that a large per cent of excitatory neurons in PER/ECT show a long latency for spike generation that might contribute to gating of inputs and to temporal integration (Beggs et al., 2000; Faulkner & Brown, 1999; Kajiwara & Tominaga, 2021; Storm, 1988). These features of the excitatory population might not require the fast membrane properties that characterize fast-spiking neurons in sensory cortices.

Variations of the morpho-electrical properties of neuron types and their circuits have been described within cortical areas (Fletcher & Williams, 2019; Large et al., 2018). Other studies have highlighted the distribution of specific cell types across cortical areas, pinpointing at regional specializations (Scala et al., 2019). These studies and our results suggest the importance of investigating the biogeography of cortical neurons to understand the circuits underlying region-specific computations.

The expression of PV in the cortex increases throughout the first three postnatal weeks (Goldberg et al., 2011), and it has been shown to be activity dependent (Donato et al., 2013). All our experiments were performed on adult mice (>2 month), a time when the pattern of PV expression has already been established. Upregulation of PV in neurons with low levels of PV expression has been demonstrated in the hippocampus of mice upon training on a task (Donato et al., 2013). However, it has never been assessed whether this occurs in GABAergic neurons that do not express PV. Future studies should address how network activity interacts with PV expression in the two populations of fast-spiking neurons in association areas. Interestingly, rat models of temporal lobe epilepsy show a reduced number of PV-INs (Benini et al., 2011). The loss of PV expression in epileptic tissue might be due to a loss of expression of PV rather than to cell death of PV-INs (Filice et al., 2016; Medici et al., 2016). The lack of PV expression in a large population of fast-spiking neurons in association areas suggests that these areas might be more prone to seizures (Biagini et al., 2013). The intersectional strategy described here could provide a tool to manipulate the activity of these neurons in epilepsy models to unveil their contribution to seizure generation.

Modelling studies showed that the density of PV-INs across cortical areas is tightly correlated with a connectivity based hierarchical organization of the cortex (Ding et al., 2024; Kim et al., 2017). These studies assumed that the low density of fast-spiking neurons in association areas and the circuit motifs of the cortex promote disinhibition of the excitatory population and increased recurrency in these cortices (Ding et al., 2024; Kim et al., 2017). However, our results demonstrate that the density of fast-spiking neurons comparable across cortical areas and suggest that other mechanisms might underly recurrency in association cortices. These modelling studies also suggest that inhibition from SST-INs onto fast-spiking neurons is fundamental in establishing recurrent activity in association cortices. Future studies might test whether fast-spiking neurons in association cortices receive stronger inputs from SST-INs, which might promote recurrency as suggested by previous modeling studies (Ding et al., 2024; Kim et al., 2017).

5 | LIMITATIONS OF THE STUDY

We acknowledge that proving a negative is very hard because the fast-spiking neurons not expressing PV we describe here might have very low levels of PV, below the threshold for detection with immunofluorescence, or PV might have been dialyzed in the cells recorded with whole-cell patch clamp. However, the per cent of fast-spiking neurons in PER in the GAD67-GFP line is undeniably higher than expected from PV expression in the same mouse line. This suggests that a much higher density of these neurons is present in association cortices as compared with what expected from quantification that relied on the PV-cre mouse line (Kim et al., 2017;

Whissell et al., 2015). Moreover, in situ hybridization for PV in the mouse brain performed by the Allen Brain Institute confirmed that PV expressing neurons are fewer in association areas (Lein et al., 2006) (Figure S3). Independently of the detectability of PV expression, our study reveals a major component of the fast-spiking population that was previously unacknowledged.

AUTHOR CONTRIBUTIONS

Erik Justin Courcelles: investigation, data curation, formal analysis, writing – review & editing; **Kasper Kjelsberg**: investigation, data curation, formal analysis, writing – review & editing; **Laura Convertino**: investigation, formal analysis; **Rajeevkumar Raveendran Nair**: resources, writing – review & editing; **Menno P. Witter**: funding acquisition, writing – review & editing; **Maximiliano José Nigro**: conceptualization, methodology, investigation, data curation, formal analysis, validation, visualization, project administration, supervision, funding acquisition, writing – original draft, writing – review & editing.

ACKNOWLEDGEMENTS

We thank Dr. Grethe Olsen for excellent technical assistance and all members of the Nigro group at the Kavli Institute for Systems Neuroscience for constructive criticism. We also thank Dr. Bernardo Rudy, Dr. Robert Machold and Dr. Hector Zurita for their comments on an earlier version of this manuscript. This research was funded by the Norwegian Research Council through the Center of Excellence scheme – Center for Neural Computation (Grant No. 223262 to MPW) and Center for Algorithms in the Cortex (Grant No. 332640 to MJN), the European Union's Horizon 2020 Research and Innovation Programme under the Marie Skłodowska-Curie (Grant No. 885955 to MJN) and the Kavli Foundation.

CONFLICT OF INTEREST STATEMENT

The authors declare no conflict of interest.

PEER REVIEW

The peer review history for this article is available at https://www.webofscience.com/api/gateway/wos/peer-review/10.1111/ejn.16341.

DATA AVAILABILITY STATEMENT

All data generated for this study are available from the corresponding author upon request. All dataset generated for this study are available as Supplemental Information to the manuscript. These include all histological quantifications and the electrophysiological properties of fast-spiking neurons in PER and wS1.

REFERENCES

Anastasiades, P. G., Marlin, J. J., & Carter, A. G. (2018). Cell-type specificity of callosally evoked excitation and feedforward inhibition in the prefrontal cortex. *Cell Reports*, *22*, 679–692. https://doi.org/10.1016/j.celrep.2017.12.073

Beaudin, S. A., Singh, T., Agster, K. L., & Burwell, R. (2013). Borders and comparative cytoarchitecture of the perirhinal and postrhinal cortices in an F1 hybrid mouse. *Cerebral Cortex*, *23*(2), 460–476. https://doi.org/10.1093/cercor/bhs038

Beggs, J. M., Moyer, J. R. Jr., McGann, J. P., & Brown, T. H. (2000). Prolonged synaptic integration in perirhinal cortical neurons. *Journal of Neurophysiology*, *83*, 3294–3298. https://doi.org/10.1152/jn.2000.83.6.3294

Benini, R., Longo, D., Biagini, G., & Avoli, M. (2011). Perirhinal cortex hyperexcitability in pilocarpine-treated epileptic rats. *Hippocampus*, *21*, 702–713. https://doi.org/10.1002/hipo.20785

Biagini, G., D'Antuono, M., Benini, R., de Guzman, P., Longo, D., & Avoli, M. (2013). Perirhinal cortex and temporal lobe epilepsy. *Frontiers in Cellular Neuroscience*, *7*, 130. https://doi.org/10.3389/fncel.2013.00130

Burwell, R. D., Witter, M. P., & Amaral, D. G. (1995). Perirhinal and postrhinal cortices of the rat: A review of the neuroanatomical literature and comparison with findings from the monkey brain. *Hippocampus*, *5*(5), 390–408. https://doi.org/10.1002/hipo.450050503

de Curtis, M., & Paré, D. (2004). The rhinal cortices: A wall of inhibition between the neocortex and the hippocampus. *Progress in Neurobiology*, *74*, 101–110. https://doi.org/10.1016/j.pneurobio.2004.08.005

Ding, X., Froudist-Walsh, S., Jaramillo, J., Jiang, J., & Wang, X.-J. (2024). Cell type-specific connectome predicts distributed working memory activity in the mouse brain. *elife*, *13*, e85442. https://doi.org/10.7554/eLife.85442

Donato, F., Rompani, S. B., & Caroni, P. (2013). Parvalbumin-expressing basket-cell network plasticity induced by experience regulates adult learning. *Nature*, *504*, 272–276. https://doi.org/10.1038/nature12866

Faulkner, B., & Brown, T. H. (1999). Morphology and physiology of neurons in the rat perirhinal-lateral amygdala area. *The Journal of Comparative Neurology*, *411*, 613–642. https://doi.org/10.1002/(SICI)1096-9861(19990906)411:4<613::AID-CNE7>3.0.CO;2-U

Filice, F., Vörckel, K. J., Sungue, A. Ö., Wöhr, M., & Schwaller, B. (2016). Reduction in parvalbumin expression not loss of the parvalbumin-expressing GABA interneuron subpopulation in genetic parvalbumin and shank mouse models of autism. *Molecular Brain*, *9*, 10. https://doi.org/10.1186/s13041-016-0192-8

Fletcher, L. N., & Williams, S. R. (2019). Neocortical topology governs the dendritic integrative capacity of layer 5 pyramidal neurons. *Neuron*, *101*, 76–90. https://doi.org/10.1016/j.neuron.2018.10.048

Franklin, K. B. J., & Paxinos, G. (2007). *The mouse in stereotaxic coordinates*. Academic Press.

Gabernet, L., Jadhav, S. P., Feldman, D. E., Carandini, M., & Scanziani, M. (2005). Somatosensory integration controlled by dynamic thalamocortical feed-forward inhibition. *Neuron*, *48*, 315–327. https://doi.org/10.1016/j.neuron.2005.09.022

Goldberg, E. M., Jeong, H.-Y., Kruglikov, I., Tremblay, R., Lazarenko, R. M., & Rudy, B. (2011). Rapid developmental maturation of neocortical FS cell intrinsic excitability. *Cerebral Cortex*, *21*, 666–682. https://doi.org/10.1093/cercor/bhq138

Harris, K. D., & Shepherd, G. M. (2015). The neocortical circuit: Themes and variations. *Nature Neuroscience*, *18*, 170–181. https://doi.org/10.1038/nn.3917

Helmstaedter, M., Staiger, J. F., Sakmann, B., & Feldmeyer, D. (2008). Efficient recruitment of layer 2/3 interneurons by layer 4 input in single columns of rat somatosensory cortex. *The Journal of Neuroscience*, *28*, 8273–8284. https://doi.org/10.1523/JNEUROSCI.5701-07.2008

Kajiwara, R., & Tominaga, T. (2021). Perirhinal cortex area 35 controls the functional link between the perirhinal and entorhinal-hippocampal circuitry: D-type potassium channel-mediated gating of neural propagation from the perirhinal cortex to the entorhinal-hippocampal circuitry. *BioEssays*, *43*, e2000084. https://doi.org/10.1002/bies.202000084

Kepecs, A., & Fishell, G. (2014). Interneuron cell types are fit to function. *Nature*, *505*, 318–326. https://doi.org/10.1038/nature12983

Kim, Y., Yang, G. R., Pradhan, K., Venkataraju, K. U., Bota, M., Del Molino, L. C. G., Fitzgerald, G., Ram, K., He, M., Levine, J. M., Mitra, P., Huang, Z. J., Wang, X.-J., & Osten, P. (2017). Brain-wide maps reveal stereotyped cell-type-based cortical architecture and subcortical sexual dimorphism. *Cell*, *171*, 456–469. https://doi.org/10.1016/j.cell.2017.09.020

Large, A. M., Vogler, N. W., Canto-Bustos, M., Friason, F. K., Schick, P., & Oswald, A.-M. M. (2018). Differential inhibition of pyramidal cells and inhibitory interneurons along the rostro-caudal axis of anterior piriform cortex. *Proceedings of the National Academy of Sciences USA*, *115*, E8067–E8076. https://doi.org/10.1073/pnas.1802428115

Lee, S., Hjerling-Leffler, J., Zagha, E., Fishell, G., & Rudy, B. (2010). The largest group of superficial neocortical GABAergic interneurons expresses ionotropic serotonin receptors. *The Journal of Neuroscience*, *30*, 16796–16808. https://doi.org/10.1523/JNEUROSCI.1869-10.2010

Lein, E. S., Hawrylycz, M. J., Ao, N., Ayres, M., Bensinger, A., Bernard, A., Boe, A. F., Boguski, M. S., Brockway, K. S., Byrnes, E. J., Chen, L., Chen, L., Chen, T. M., Chin, M. C., Chong, J., Crook, B. E., Czaplinska, A., Dang, C. N., Datta, S., … Jones, A. R. (2006). Genome-wide atlas of gene expression in the adult mouse brain. *Nature*, *445*, 168–176. https://doi.org/10.1038/nature05453

Luo, L. (2021). Architectures of neuronal circuits. *Science*, *373*, eabg7285. https://doi.org/10.1126/science.abg7285

Ma, Y., Hu, H., Berrebi, A. S., Mathers, P. H., & Agmon, A. (2006). Distinct subtypes of somatostatin-containing neocortical interneurons revealed in transgenic mice. *The Journal of Neuroscience*, *26*, 5069–5082. https://doi.org/10.1523/JNEUROSCI.0661-06.2006

McGarry, L. M., & Carter, A. G. (2016). Inhibitory gating of basolateral amygdala inputs to the prefrontal cortex. *The Journal of Neuroscience*, *36*, 9391–9406. https://doi.org/10.1523/JNEUROSCI.0874-16.2016

Medici, V., Rossini, L., Deleo, F., Tringali, G., Tassi, L., Cardinale, F., Bramerio, M., de Curtis, M., Garbelli, R., & Spreafico, R. (2016). Different parvalbumin and GABA expression in human epileptogenic focal cortical dysplasia. *Epilepsia*, *57*, 1109–1119. https://doi.org/10.1111/epi.13405

Nigro, M. J., Hashikawa-Yamasaki, Y., & Rudy, B. (2018). Diversity and connectivity of layer 5 somatostatin-expressing interneurons in the mouse barrel cortex. *The Journal of Neuroscience*, *38*, 1622–1633. https://doi.org/10.1523/JNEUROSCI.2415-17.2017

Nigro, M. J., Kirikae, H., Kjelsberg, K., Nair, R. R., & Witter, M. P. (2021). Not all that is gold glitters: PV-IRES-Cre mouse line shows low efficiency of labeling of parvalbumin interneurons in the perirhinal cortex. *Frontiers in Neural Circuits*, *15*, 781928. https://doi.org/10.3389/fncir.2021.781928

Pitkänen, A., & Amaral, D. G. (1993). Distribution of parvalbumin-immunoreactive cells and fibers in the monkey temporal lobe: The hippocampal formation. *The Journal of Comparative Neurology*, *331*, 37–74. https://doi.org/10.1002/cne.903310104

Pouille, F., & Scanziani, M. (2001). Enforcement of temporal fidelity in pyramidal cells by somatic feed-forward inhibition. *Science*, *293*, 1159–1163. https://doi.org/10.1126/science.1060342

Raudales, R., Kim, G., Kelly, S. M., Hatfield, J., Guan, W., Zhao, S., Paul, A., Qian, Y., Li, B., & Huang, Z. J. (2023). Specific and comprehensive genetic targeting reveals brain-wide distribution and synaptic input patterns of GABAergic axo-axonic interneurons. *bioRxiv*. 11.07.5666059. https://doi.org/10.1101/2023.11.07.566059

Rudy, B., Fishell, G., Lee, S., & Hjerling-Leffler, J. (2011). Three groups of interneurons account for nearly 100% of neocortical GABAergic neurons. *Developmental Neurobiology*, *71*, 45–61. https://doi.org/10.1002/dneu.20853

Scala, F., Kobak, D., Shan, S., Bernaerts, Y., Laturnus, S., Cadwell, C. R., Hartmanis, L., Froudarakis, E., Castro, J. R., Tan, Z. H., Papadopoulos, L., Patel, S. S., Sandberg, R., Berens, P., Jiang, X., & Tolias, A. S. (2019). Layer 4 of mouse neocortex differs in cell types and circuit organization between sensory areas. *Nature Communications*, *10*, 1–12.

Storm, J. F. (1988). Temporal integration by a slowly inactivating K + current in hippocampal neurons. *Nature*, *336*, 379–381. https://doi.org/10.1038/336379a0

Tamamaki, M., Yanagawa, Y., Tomioka, R., Miyazaki, J., Obata, K., & Kaneko, T. (2003). Green fluorescent protein expression and colocalization with calretinin, parvalbumin and somatostatin in the GAD67-GFP knock-in mouse. *The Journal of Comparative Neurology*, *467*, 60–79. https://doi.org/10.1002/cne.10905

Taniguchi, H., Lu, J., & Huang, Z. J. (2013). The spatial and temporal origin of chandelier cells in mouse neocortex. *Science*, *339*, 70–74. https://doi.org/10.1126/science.1227622

Tasic, B., Menon, V., Nguyen, T. N., Kim, T. K., Jarsky, T., Yao, Z., Levi, B., Gray, L. T., Sorensen, S. A., Dolbeare, T., Bertagnolli, D., Goldy, J., Shapovalova, N., Parry, S., Lee, C., Smith, K., Bernard, A., Madisen, L., Sunkin, S. M., … Zeng, H. (2016). Adult mouse cortical cell taxonomy revealed by single cell transcriptomics. *Nature Neuroscience*, *19*, 335–346. https://doi.org/10.1038/nn.4216

Tasic, B., Yao, Z., Graybuck, L. T., Smith, K. A., Nguyen, T. N., Bertagnolli, D., Goldy, J., Garren, E., Economo, M. N., Viswanathan, S., Penn, O., Bakken, T., Menon, V., Miller, J., Fong, O., Hirokawa, K. E., Lathia, K., Rimorin, C., Tieu, M., … Zeng, H. (2018). Shared and distinct transcriptomic cell types

across neocortical areas. *Nature*, *563*, 72–78. https://doi.org/10.1038/s41586-018-0654-5

Tremblay, R., Lee, S., & Rudy, B. (2016). GABAergic interneurons in the neocortex: From cellular properties to circuits. *Neuron*, *91*, 260–292. https://doi.org/10.1016/j.neuron.2016.06.033

Uva, L., Grüschke, S., Biella, G., De Curtis, M., & Witter, M. P. (2004). Cytoarchitectonic characterization of the parahippocampal region of the Guinea pig. *The Journal of Comparative Neurology*, *474*, 289–303. https://doi.org/10.1002/cne.20121

van Brederode, J., Helliesen, M., & Hendrickson, A. (1991). Distribution of the calcium-binding proteins parvalbumin and calbindin-D28k in the sensorimotor cortex of the rat. *Neuroscience*, *44*, 157–171. https://doi.org/10.1016/0306-4522(91)90258-P

van de Werd, H. J. J. M., Rajkowska, G., Evers, P., & Uylings, H. B. M. (2010). Cytoarchitectonic and chemoarchitectonic characterization of the prefrontal cortical areas in the mouse. *Brain Structure & Function*, *214*, 339–353. https://doi.org/10.1007/s00429-010-0247-z

van Essen, D. C., & Glasser, M. F. (2018). Parcellating cerebral cortex: How invasive animal studies inform noninvasive mapmaking in humans. *Neuron*, *99*, 640–663. https://doi.org/10.1016/j.neuron.2018.07.002

Vormstein-Schneider, D., Lin, J. D., Pelkey, K. A., Chittajallu, R., Guo, B., Arias-Garcia, M. A., Allaway, K., Sakopoulos, S., Schneider, G., Stevenson, O., Vergara, J., Sharma, J., Zhang, Q., Franken, T. P., Smith, J., Ibrahim, L. A., Mastro, K. J., Sabri, E., Huang, S., … Dimidschstein, J. (2020). Viral manipulation of functionally distinct interneurons in mice, non-human primates and humans. *Nature Neuroscience*, *23*, 1629–1636. https://doi.org/10.1038/s41593-020-0692-9

Whissell, P. D., Cajanding, J. D., Fogel, N., & Kim, J. C. (2015). Comparative density of CCK-and PV-GABA cells within the cortex and hippocampus. *Frontiers in Neuroanatomy*, *9*, 124. https://doi.org/10.3389/fnana.2015.00124

Willems, J. G., Wadman, W. J., & Cappaert, N. L. (2018). Parvalbumin interneuron mediated feedforward inhibition controls signal output in the deep layers of the perirhinal-entorhinal cortex. *Hippocampus*, *28*, 281–296. https://doi.org/10.1002/hipo.22830

Xu, X., Roby, K. D., & Callaway, E. M. (2010). Immunochemical characterization of inhibitory mouse cortical neurons: Three chemically distinct classes of inhibitory cells. *The Journal of Comparative Neurology*, *518*, 389–404. https://doi.org/10.1002/cne.22229

SUPPORTING INFORMATION

Additional supporting information can be found online in the Supporting Information section at the end of this article.

How to cite this article: Courcelles, E. J., Kjelsberg, K., Convertino, L., Nair, R. R., Witter, M. P., & Nigro, M. J. (2024). Association cortical areas in the mouse contain a large population of fast-spiking GABAergic neurons that do not express parvalbumin. *European Journal of Neuroscience*, 1–20. https://doi.org/10.1111/ejn.16341